DENTAL MATERIALS 24 (2008) 715–723

available at www.sciencedirect.com

ScienceDirect

journal homepage: www.intl.elsevierhealth.com/journals/dema

Magnetic susceptibility and electrical conductivity of metallic dental materials and their impact on MR imaging artifacts

Jana Starčuková[a,*], *Zenon Starčuk Jr.*[a], *Hana Hubálková*[b], *Igor Linetskiy*[b]

[a] *Institute of Scientific Instruments of the ASCR, v.v.i., Academy of Sciences of the Czech Republic, Královopolská 147, 612 64 Brno, Czech Republic*

[b] *Charles University, First Medical Faculty, Department of Stomatology, Prague, Czech Republic*

ARTICLE INFO

Article history:
Received 5 January 2007
Received in revised form
31 July 2007
Accepted 31 July 2007

Keywords:
Metallic dental materials
Dental alloys
Amalgams
MR imaging
Magnetic susceptibility
Electric conductivity
Image artifact

ABSTRACT

Objectives. The aim of this study was to test the hypothesis that dental materials vary significantly in MR-relevant material parameters—magnetic susceptibility and electrical conductivity, and that knowledge of these parameters may be used to estimate the quality of MR imaging in the presence of devices made of such materials.

Methods. Magnetic susceptibility, electrical conductivity and artifacts were evaluated for 45 standardized cylindrical samples of dental alloys and amalgams. Magnetic susceptibility was determined by fitting the phase of gradient-echo MR images to numerically modeled data. Electrical conductivity was determined by standard electrotechnical measurements. Artifact sizes were measured in spin-echo (SE) and gradient-echo (GE) images at 1.5 T according to the standards of the American Society for Testing and Materials.

Results. It has been confirmed that dental materials differ considerably in their magnetic susceptibility, electrical conductivity and artifacts. For typical dental devices, magnetic susceptibility differences were found of little clinical importance for diagnostic SE/GE imaging of the neck and brain, but significant for orofacial imaging. Short-TE GE imaging has been found possible even in very close distances from dental devices made of amalgams, precious alloys and titanium alloys. Nickel–chromium and cobalt–chromium artifacts were found still acceptable, but large restorations of aluminum bronzes may preclude imaging of the orofacial region. The influence of electrical conductivity on the artifact size was found negligible.

Significance. MR imaging is possible even close to dental devices if they are made of dental materials with low magnetic susceptibility. Not all materials in current use meet this requirement.

1. Introduction

The increasing number of indications for magnetic resonance imaging (MRI) examination of the head and neck regions is associated with a growing number of patients with metal devices present in the orofacial area, such as dental crowns, fixed bridges, splints and implants, surgical fixtures and clips. While MR examination is a very useful noninvasive imaging

* *Corresponding author.* Tel.: +420 541 514 247; fax: +420 541 514 402.
E-mail address: jana@isibrno.cz (J. Starčuková).

0109-5641/$ – see front matter © 2007 Academy of Dental Materials. Published by Elsevier Ltd. All rights reserved.
doi:10.1016/j.dental.2007.07.002

method, it may pose a risk for a patient with a metallic dental device and/or it may provide confusing results due to artifacts caused (i) by the static field inhomogeneity arising from the difference in the magnetic susceptibility of the dental device and the observed tissue [1,2] and (ii) by varying magnetic fields arising from eddy currents induced in a conductive device by the excitation radio frequency (RF) field [3,4] or switched gradient fields [5]. Thus, it may be possible to use magnetic susceptibility and electrical conductivity of a material as indicators of the impact of the material on the arising MR artifact, which, however, further depends on the device shape and orientation, the static magnetic field strength and the pulse sequence type (echo type, dimensionality) and parameters (such as gradient pulse amplitudes, echo time, volume-of-interest position and orientation). Magnetic and conductive materials also raise safety concerns; investigation of MR safety aspects of metallic dental materials is, however, beyond of the scope of this paper. MR compatibility is becoming particularly important as the use of clinical high-field scanners (operating mostly at 3 T) are gaining ground.

The information about magnetic susceptibility and electrical conductivity is not readily available for most of the materials used in dentistry. To the authors' knowledge, correlation between susceptibility and spin echo image disturbance has been studied for dental alloys of precious metals only [6] and no comparative study has been performed for a wider range of metallic dental materials. Some studies [7,8] report differences in the artifact sizes caused by the presence of metallic dental materials in the oral cavity. While the absence of artifacts has been reported for amalgams, restorations from precious alloys and titanium implants [9,10], large image deformations have been found with non-precious alloys [7]. Differences in artifact sizes, magnetic susceptibilities and electrical conductivities of various metallic dental materials have been observed in the authors' preliminary study [8,11], but no standardized measurement of artifacts and their comparison with MR-relevant material parameters has been performed.

The aim of this study was to measure the magnetic susceptibility and the electrical conductivity of metallic dental materials in current use, to quantify the MRI artifacts found in images measured with standardized samples by standard pulse sequences and, ultimately, to support the preference of more MR-compatible materials by providing dentists and dental material manufactures with indications concerning the MR-relevant dental material parameters.

2. Materials and methods

2.1. Metallic dental materials

Cylindrical samples, 4 mm in diameter and 20 mm in height, were cast according to the instructions of manufacturers of 45 commercially available amalgams and dental alloys: high-noble, noble (gold and palladium based) and predominantly base metal alloys (titanium, aluminum bronze, cobalt–chromium and nickel–chromium alloys). The names, the manufacturers and the compositions of the metallic dental materials examined are listed in Table 1.

2.2. Determination of magnetic susceptibility

MRI measurements were used to determine the dimensionless volume magnetic susceptibility χ on a 1.5-T whole-body scanner (MAGNETOM Symphony, Siemens AG, Germany). Each cylindrical sample was placed in a polymethyl methacrylate (PMMA) holder in parallel with the static magnetic field B_0 and immersed in a $CuSO_4$ solution (1.25 g/L) with susceptibility close to water ($\chi_{water} = -9.05 \times 10^{-6}$), closely approximating the susceptibility of human tissues. 2D gradient echo images with suitable echo times (TE) were taken from 2 mm-thick slices perpendicular to the static magnetic field B_0 and set to intersect the sample in the middle. Echo-time TE = 6 ms was selected for aluminum bronzes with the largest artifacts, TE = 10 ms was used for all other non-precious alloys, and TE = 40 ms for amalgams and alloys of precious metals with the smallest artifacts. Reference images were taken from the same location. The slice selection gradient of 20 mT/m (850 Hz/mm) was sufficient to limit the central slice deviation to less than 2 mm (4 mm for aluminum bronzes), which was confirmed to be true and negligible by numerical modeling and by imaging of orthogonal slices. The readout-direction distortion could not be neglected with the gradient of 15.5 mT/m (661 Hz/mm, used for measurements with TE = 6 ms) or 6 mT/m (256 Hz/mm, used with TE of 10 and 40 ms) and was taken care of in data evaluation [8]. Unwrapped phase images were used for the construction of B_0 inhomogeneity maps. The field distortion due to the sample was calculated by subtracting the field maps acquired with and without the material sample. These data were compared with the results of a numerical model based on the Fourier-domain field calculation [12,13]. The values of difference magnetic susceptibility $\Delta\chi = \chi - \chi_{water}$ were found by least-squares fitting. Field map calculations and fitting were accomplished in Matlab (The MathWorks Inc., USA).

2.3. Determination of electrical conductivity

The electrical conductivity σ (S/m)was determined by a standard electrotechnical measurement. The cylinder under test was connected by copper contacts to a current circuit with a dc current supply ($I = 2$ A, stability 2×10^{-3}) and an ammeter. Voltage drop U (V) was measured using two test clips attached to the cylinder $l = 14$ mm apart. The electrical conductivity was calculated from $\sigma = 4Il/(\pi d^2 U)$.

2.4. Assessment of artifacts

For the measurement of the artifacts the ASTM F2119-01 standard [14] was used. A cylindrical sample was placed into a PMMA holder and immersed in a $CuSO_4$ solution (1.25 g/L) at the center of a box-shaped phantom made of PMMA with the inner dimensions of 100 mm × 100 mm × 100 mm. Three cylindrical PMMA bars were positioned inside the cube near its edges for reference. Imaging was performed with a Siemens Magnetom Symphony 1.5-T whole-body scanner.

Artifacts were measured for all the materials examined with the exception of alloys of precious metals made by C Hafner, which were not available at the time of measure-

Table 1 – List of metallic dental materials tested

Brand name	Manufacturer	Composition with mass (%)
Amalgams		
Starfill NG2	Ogussa (Austria)	Ag 70, Cu 15, Hg 3, Sn 12
Ana 2000 Duet	Nordiska Dental (Sweden)	Ag 43, Cu 25.4, Hg 2, Sn 29.6
Safargam Plus	Safina (Czech Republic)	Ag 50, Cu 20.1, Sn 29.9
Safargam NG2	Safina (Czech Republic)	Ag 42, Cu 26.5, Sn 31.5
Safargam Special	Safina (Czech Republic)	Ag 69.4, Cu 4.6, Sn 26
Ana 70 Duett	Nordiska Dental (Sweden)	Ag 69.3, Cu 10.9, Sn 19.4, Zn 0.4
Precious alloys		
Aurosa	Safina (Czech Republic)	Ag 44.8, Au 20, Cu 14.4, Pd 20, Zn <1
Pangold Keramik N2	C Hafner (Germany)	Ag 20, Au 15, Ga 1, In 6, Pd 52.3, Pt 0.1, Re 0.1, Sn 5.5
Au 18 kar Pt	Safina (Czech Republic)	Ag 8.3, Au 74.3, Cu 11.4, Pt 6
Argenpal IV A	Safina (Czech Republic)	Ag 59.9, Au 5, Cu 10, Ir <1, Pd 22.5, Sn <1, Zn 2
Palargen L	Safina (Czech Republic)	Ag 57.5, Pd 40, Sn <1, Zn 2.1
Aurix L 60	Safina (Czech Republic)	Ag 26, Au 54.5, Cu 12, Pd 5, Pt <1, Zn 2
Pangold	C Hafner (Germany)	Ag 59, Au 5, Cu 12, Pd 23, Zn 1
Koldan	Safina (Czech Republic)	Ag 89.9, Sn 9.3, Zn <1
Aurix L	Safina (Czech Republic)	Ag 20, Au 65.1, Cu 9.6, Pd 3, Pt 1.3, Zn 1
Orplid Keramik PF	C Hafner (Germany)	Au 77.7, Ir 0.1, Pt 19.5, Ru 0.4, Ta 0.3, Zn 2
Orplid Keramik 4	C Hafner (Germany)	Ag 1.7, Au 74.5, Cu 0.1, In 2.9, Ir 0.1, Pd 10, Pt 10.2, Sn 0.5, Re 0.1
Safibond Bio	Safina (Czech Republic)	Ag 2, Au 77.6, Ir <1, Pt 18, Ti <1, Zn 1.8
Orplid Keramik 3	Hafner (Germany)	Ag 0.5, Au 84, Cu 0.1, In 2.4, Ir 0.1, Pd 4.7, Pt 8.2
Safibond Plus	Safina (Czech Republic)	Au 78, Ir <1, Pd 6.8, Pt 11.5
Orplid Keramik 5	Hafner (Germany)	Au 86.2, Mn 0.1, Pt 11.5, Zn 1.5
Orplid Keramik 2	Hafner (Germany)	Au 87.5, Fe 0.5, In 1, Pt 11
Ti		
Biotan	Schütz-Dental Group (Germany)	C <0.1, Fe <0.2, Ti 99.5
Titanium soft	NA	NA
Titanium hard	NA	NA
Titanium Gr2	Orotig (Italy)	Ti 99.78
Ni–Cr–Mo		
I-Bond 02	Interdent (Slovenia)	Ce 0.3, Cr 22.6, Fe 0.5, Mo 9.6, Nb 1, Ni 65, Si 1
Wiron 99	Bego (Germany)	C <0.02, Ce 0.5, Cr 22.5, Fe 0.5, Mo 9.5, Nb 1, Ni 65, Si 1
Remanium GW	Dentaurum (Germany)	Cr 20.5, Mo 5, Ni 66, Si 1.5
Wirolloy	Bego (Germany)	C <0.1, Cr 23, Fe 9, Mo 3, Ni 63.2, Si 1.8
Non-precious alloys Co–Cr		
Duceralloy	Degussa (Germany)	Co 60, Cr 25, W 9
I-Bond NF	Interdent (Slovenia)	Co 63, Cr 24, Mo 3, Nb 1, Si 1, W 8
Remanium Star	Dentaurum (Germany)	Co 60.5, Cr 28, Si 1.5, W 9
Remanium GM800	Dentaurum (Germany)	Co 63.3, Cr 30, Mo 5, (C, Mn, N, Si)
I-MG	Interdent (Slovenia)	C 0.3, Co 62.5, Cr 29.5, Mn 0.6, Mo 5.5, Si 1.4
Wirobond C	Bego (Germany)	C <0.02, Ce 0.5, Co 61, Cr 26, Fe 0.5, Mo 6, Si 1, W 5
Oralium Ceramic	Safina (Czech Republic)	Co 61, Cr 26, Fe <2, Mn <2, Mo 6, Si <2, W 5
BNF2000	Elephant Industries BV (Netherlands)	Co 65.8, Cr 20, Mo 6, W 6, (Fe, Mn, Ni, Si)
Wironit	Bego (Germany)	C <0.35, Co 64, Cr 28.65, Mn <0.35, Mo 5, Si <0.35
Sheradent	Shera W-T (Germany)	Co 67, Cr 21, Mo 6, W 6
Brealloy C + B270	Bredent (Germany)	Co 66, Cr 20, Mo 6, Si 0.9, W 6, (C, Mn)
Oralium	Safina (Czech Republic)	C <2, Co 63.5, Cr 28.5, Fe <2, Mn <2, Mo 5.8, Si <2
Al–Cu–Ni		
Orcast	Madespa (Spain)	Al 9.5, Cu 83.5, Ni 5, (Fe)
Orcast plus	Madespa (Spain),	Al 7, Cu 83, Ni 5, (Fe)
NPG	Aalba Dent Inc. (USA)	Al 7.8, Cu 80.7, Fe 3, Mn 1.7, Ni 4.3, Zn 2.7

ment. First, four selected samples (Titanium Gr2, Oralium, Orcast and NPG) were tested in parallel and perpendicular orientations with respect to the static magnetic field B_0 using standard pulse sequences (bandwidth 32 kHz, field of view 120 mm × 120 mm, matrix size 256 × 256, slice thickness 3 mm). Multislice turbo spin echo (SE) sequence with TR = 3000 ms, TE = 15 ms and the refocusing pulse flip angle of 180°, and gradient echo (GE) sequences with TR = 200 ms, TE = 10 ms and the flip angle of 35° were used for all measurements. Multiple "sagittal" slices (assuming head-first supine patient orientation), covering the extent of the artifact, were acquired with and without the sample using both possibilities of assignment of readout and phase-encode directions.

For the determination of the artifact extent, defined as the distance (mm) from the cylinder boundary to the fringe of the artifact, Marevisi (software for MRI and MRSI data visualization and processing by Institute for Biodiagnostics, NRC, Canada) was used. To measure the artifact, a rectangular region of interest (ROI) centered at the image center and enclosing the whole artifact was selected first. Then, the mean intensity of the reference image in the same ROI was determined and the test image intensity thresholds were set to values 30% above and below this value, making all pixels with intensities beyond the thresholds black or white. Using the knowledge of the dimensions of the cylindrical sample and its position relative to the reference cylinders, a circle or rectangle (depending on the sample orientation with respect to the static magnetic field B_0) was drawn into the exact position of the sample in the image. The measurement tools of Marevisi were used to find the distance between the sample boundary and the fringe of the artifact. The maximum distance found in the entire set of images was finally used to characterize the artifact size in spin echo and gradient echo images.

For all other samples the measurement was limited to acquiring "sagittal" slices perpendicular to the sample cylinders, using vertical (PA) readout direction for both SE and GE, since this combination was found always to give the maximal artifact extent for all the tested cylinders.

3. Results

Differences in magnetic susceptibilities with 95% confidence intervals, electrical conductivities and maximal extents of artifacts for GE and SE are listed in Table 2. None of the materials tested was found to be ferromagnetic. Nevertheless, considerable differences in magnetic susceptibility, electrical conductivity and artifact extents have been found even among materials of a similar chemical composition (Fig. 1). For GE, the relationship between magnetic susceptibility of a metallic dental material and the extent of the corresponding MRI artifact is displayed in Fig. 2 .

3.1. *Amalgams and alloys of precious metals*

No significant differences were found between the amalgams studied. All of them were found to be diamagnetic, with low difference susceptibilities in a very narrow range of -17.5×10^{-6} to -29.6×10^{-6}. Their conductivities are between 3.24 MS/m and 4.13 MS/m. The artifacts extended to only 4.3–4.9 mm for GE and 2.6–3.4 mm for SE from the cylinder surface.

Alloys of precious metals, characterized in most cases by very low negative difference in magnetic susceptibility (between -10.6×10^{-6} and -24.4×10^{-6}) and small artifacts (3.4–4.3 mm for GE and 2.3–3.4 mm for SE), vary greatly in their electrical conductivity (2.55–9.41 MS/m). In the single case of Orplid Keramik 2, marked by the presence of a low amount of iron, an elevated difference in magnetic susceptibility of 189.5×10^{-6} has been found. Orplid Keramik 5 turned out to be only slightly paramagnetic.

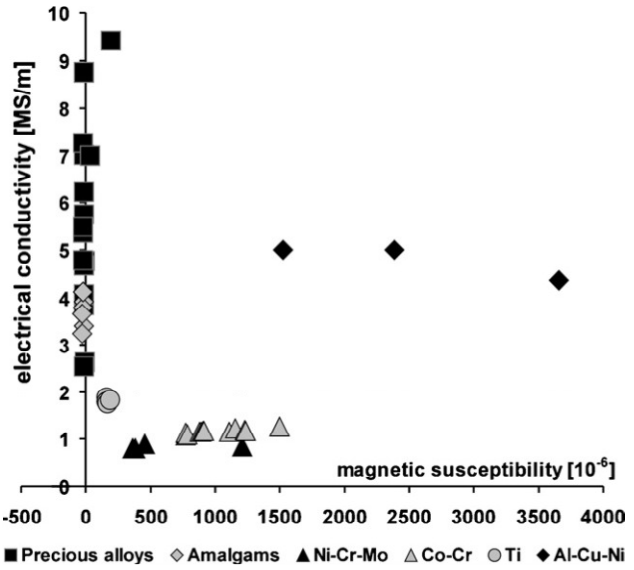

Fig. 1 – Comparison of the MR-relevant physical properties of metallic dental materials. For each material tested, a mark indicates its electrical conductivity and magnetic susceptibility as measured in this study. Materials with low values of both parameters are preferable, but according to our measurements in the 1.5 T-clinical system, low susceptibility matters most.

3.2. *Non-precious alloys*

No significant differences were found between titanium-based alloys. Their difference in magnetic susceptibilities

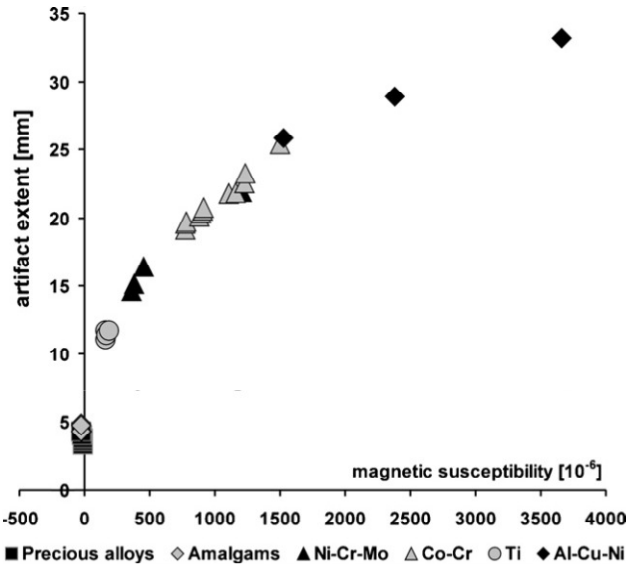

Fig. 2 – The relationship between magnetic susceptibility and the extent of the arising MRI artifact, as determined with standardized cylindrical metallic dental material samples immersed in $CuSO_4$-doped water, oriented perpendicularly to the static magnetic field B_0, and a standard gradient-echo imaging pulse sequence (TR = 200 ms, TE = 10 ms, "sagittal" slice orientation, vertical (PA) readout direction). The data follow from Table 2.

Table 2 – Difference magnetic susceptibility, electrical conductivity and artifact size determined for the metallic dental materials tested

Brand name	$\Delta\chi$ (10^{-6})	σ (MS/m)	d_{GE} (mm)	d_{SE} (mm)
Amalgams				
Starfill NG2	−17.5 (−17.8, −17.1)	3.41	–	–
Ana 2000 Duet	−17.9 (−18.3, −17.4)	3.92	–	–
Safargam Plus	−22.4 (−23.1, −21.7)	3.79	4.3	2.6
Safargam NG2	−23.7 (−24.5, −23.0)	4.13	4.3	3.1
Safargam Special	−29.4 (−29.9, −28.8)	3.24	4.9	3.3
Ana 70 Duett	−29.6 (−30.0, −29.1)	3.67	4.9	3.4
Precious alloys				
Aurosa	−10.6 (−10.9, −10.3)	4.77	3.4	2.3
Pangold Keramik N2	−12.2 (−12.5, −12.0)	2.63	–	–
Au 18 kar Pt	−12.6 (−13.0, −12.2)	3.85	3.6	2.4
Argenpal IV A	−13.4 (−13.7, −13.1)	6.23	3.7	2.5
Palargen L	−13.5 (−13.8, −13.1)	4.07	3.6	2.4
Aurix L 60	−13.8 (−14.4, −13.2)	7.02	3.8	2.5
Pangold	−15.9 (−16.1, −15.6)	8.76	–	–
Koldan	−16.0 (−16.4, −15.6)	2.55	3.8	2.7
Aurix L	−16.5 (−16.8, −16.2)	5.75	3.8	2.9
Orplid Keramik PF	−16.5 (−16.8, −16.3)	4.67	–	–
Orplid Keramik 4	−20.0 (−20.3, −19.7)	4.78	–	–
Safibond Bio	−20.5 (−21.2, −19.8)	5.37	4.1	3.2
Orplid Keramik 3	−22.8 (−23.3, −22.4)	7.27	–	–
Safibond Plus	−24.4 (−25.3, −23.5)	5.49	4.3	3.4
Orplid Keramik 5	28.7 (27.9, 29.6)	6.99	–	–
Orplid Keramik 2	189.5 (188.4, 190.7)	9.41	–	–
Ti				
Biotan	156.9 (155.8, 157.9)	1.89	11.1	9.2
Titanium soft	160.5 (158.8, 162.3)	1.75	11.4	9.8
Titanium hard	164.7 (163.1, 166.0)	1.79	11.7	10.1
Titanium Gr2	188.9 (185.9, 191.9)	1.84	11.7	10.0
Ni–Cr–Mo				
I-Bond 02	358.1 (356.5, 359.7)	0.81	14.7	13.6
Wiron 99	378.5 (376.7, 380.3)	0.80	15.1	13.4
Remanium GW	456.6 (455.3, 457.8)	0.89	16.4	14.8
Wirolloy	1209.7 (1202.9, 1216.5)	0.84	21.9	24.1
Non-precious alloys (Co–Cr)				
Duresalloy	772.0 (769.6, 774.4)	1.08	19.2	18.6
I-Bond NF	772.1 (762.8, 781.4)	1.14	19.6	19.0
Remanium Star	783.0 (773.0, 792.9)	1.09	19.7	19.2
Remanium GM800	878.7 (875.2, 882.2)	1.15	20.1	18.9
I-MG	892.7 (888.2, 897.2)	1.15	20.4	19.4
Wirobond C	908.8 (905.9, 911.8)	1.18	20.6	20.2
Oralium ceramic	913.5 (908.5, 918.4)	1.18	20.8	20.1
BNF2000	1107.0 (1095.2, 1118.8)	1.15	21.7	21.9
Wironit	1157.4 (1151.0, 1163.9)	1.23	21.8	22.2
Sheradent	1228.4 (1222.5, 1234.4)	1.19	22.6	22.7
Brealloy C + B270	1234.7 (1228.0, 1241.3)	1.18	23.2	23.1
Oralium	1498.4 (1495.0, 1502.0)	1.26	25.4	27.1
Al–Cu–Ni				
Orcast	1527.1 (1519.6, 1536.4)	5.00	25.8	27.2
Orcast plus	2383.3 (2371.8, 2394.8)	5.00	28.9	31.0
NPG	3657.8 (3637.0, 3678.5)	4.35	33.2	40.3

The difference magnetic susceptibility $\Delta\chi = \chi - \chi_{water}$ was calculated as the linear regression coefficient in fitting the B_0 inhomogeneity map measured in $CuSO_4$ solution surrounding the material to the numerical model map [8,12,13]. Goodness of fit $R^2 > 0.96$ was achieved with all materials; the interval in round parenthesis denotes 95% confidence interval of the fitted coefficient $\Delta\chi \cdot \sigma$ (MS/m) denotes the conductivity, d_{GE} (mm) and d_{SE} (mm) are the maximum distances between the sample surface to the fringe of the artifact in the gradient echo and the spin echo multislice images, respectively.

ranged from 156.9×10^{-6} to 188.9×10^{-6}, electrical conductivities from 1.75 MS/m to 1.89 MS/m and artifact extents from 11.1 mm to 11.7 mm for GE and from 9.2 mm to 10.1 mm for SE.

Low conductivity from 0.8 MS/m to 0.89 MS/m was found for nickel–chromium-based alloys. With a difference in magnetic susceptibility of 358.1×10^{-6} to 456.6×10^{-6}, and 1209.7×10^{-6} for Wirolloy, the artifact extents were 14.7–21.9 mm for GE and 13.4–24.1 mm for SE.

Cobalt–chromium alloys vary significantly in their susceptibility difference from 772×10^{-6} to 1498×10^{-6}, which led to artifact extents of 19.2–25.4 mm for GE and of 18.6–27.1 mm for SE. On the contrary, their conductivity was found to be low and in a narrow range of 1.08–1.26 MS/m.

The highest differences in susceptibilities, between 1527×10^{-6} and 3658×10^{-6}, and consequently largest artifact extents, from 25.8 mm to 33.2 mm for GE and from 27.2 mm to 40.3 mm for SE, were found for aluminum bronze alloys. Their conductivities are 4.35–5.00 MS/m.

4. Discussion

4.1. *Material properties characterizing MR compatibility*

The extent of artifacts caused by metallic dental devices depends on the magnetic susceptibility and the electrical conductivity of the device, its shape and orientation in the magnetic field, its placement in the oral cavity and on numerous MR measurement parameters, related to the MR scanner specifications, the desired type of contrast, volume-of-interest, and practical experiment time limitations. Dental manufacturers and dentists, however, can impact only the device composition, stress state of its crystalline structure and, to a limited extent, its shape, size and orientation. Since the MR-relevant physical parameters of a metallic material – its magnetic susceptibility and electrical conductivity – depend on its microstructure in a complex way, the two parameters are convenient indicators of the MR quality of the material. The ideal material would have zero electrical conductivity σ (S/m) and a magnetic susceptibility identical to that of the observed tissue. As the magnetic susceptibility of most soft tissues appears to be within ±10–20% of that of water, χ_{water} [1], the ideal material for soft tissue imaging is characterized by the difference in magnetic susceptibility $\Delta\chi = \chi - \chi_{water}$ equal to zero. Non-fulfilment of this condition leads to mislocalization and signal-loss artifacts due to inhomogeneity of the static magnetic field B_0. The absence of susceptibility artifacts on teeth–water [15,16] and teeth–tongue [17] interfaces in MRI of water-based media or with tongue surrounding teeth indicates that the magnetic susceptibility of teeth may also be close to χ_{water}. Higher electrical conductivity facilitates the induction of eddy currents that may lead to artifacts due to local RF field B_1 inhomogeneity and/or due to gradient-switching induced transient B_0 inhomogeneity around metallic devices in off-isocenter positions. Radiofrequency heating, also increasing with conductivity, cannot be assessed generally without the knowledge of the specific shape and orientation of the dental device [18].

4.2. *Comments on the measurement results*

The magnetic susceptibility and electrical conductivity of 45 metallic dental materials in current use were evaluated in this study. Unlike the authors' previous study [8,11] at 4.7 T, the magnetic susceptibilities of dental materials reported here were measured in a 1.5 T whole body system and suitable echo times (TE) were selected to optimize the artifact size for various materials and the quality of the respective B_0 inhomogeneity maps. In this way, better reliability of fitting the B_0 inhomogeneity maps to the numerical model [8,12,13] was achieved. It was found that the difference in magnetic susceptibility $|\chi - \chi_{water}|$ of the observed materials ranges approximately from 11×10^{-6} to 3660×10^{-6} and the electrical conductivity from 0.8 MS/m to 9.41 MS/m. An obvious dependence of artifact extents (from 3.4 mm to 33.2 mm for GE, and from to 2.3 mm to 40.3 mm for SE) on the magnetic susceptibility has been found (Fig. 2). On the other hand, neither a clear relation between image artifacts and electrical conductivity, nor a distinct B_1-type artifact was identified in the 1.5-T measurements, unlike the preliminary work in 4.7 T [8] where a distinct B_1-type artifact linked to the orientation of the saddle coil had been observed. The difference of the 1.5-T measurements consisted mainly of a lower spatial resolution, gradients and flip angles, and usage of a circularly polarized head coil. The eddy-current effects due to the higher electrical conductivity may play some role, though, in higher fields and in MR of the jaw.

4.3. *GE versus SE*

Surprisingly, it was found that for materials with susceptibilities $|\chi - \chi_{water}| > 1100 \times 10^{-6}$ the SE artifacts extend further from the cylinder site than those obtained by GE (Fig. 3). Nevertheless, the overall artifact size is always larger for GE, although, it can be reduced by lowering TE [19] or, if possible, by aligning the device with the static magnetic field B_0. As the GE artifact volume is approximately bound to the volume in which the local phase gradient of transverse magnetization exceeds 2π per voxel size, and because the phase gradient is proportional to both TE and susceptibility, the dependence of artifact size on susceptibility depicted in Fig. 2 can also be used to estimate the dependence of the artifact size on TE. For artifact suppression it is usually recommended to use SE [19] whenever possible. However, while the signal void caused by GE is clear to interpret, the bright artifact structures in SE images may be misinterpreted because they may originate in tissues, which are close to the metal, but located far away from the position in which they appear in the image or even far away from the observed image slice [20]. Such signals, coming from locations with high B_0 inhomogeneity, are made detectable by the phase refocusing inherent in the SE technique. Geometric distortions, mostly hidden in the no-signal artifacts in most GE images, pose another interpretation problem in SE images. As slice distortion can be avoided when true 3D encoding is used [20], 3D SE and 3D GE are recommended over 2D (including multislice) imaging. GE is preferable whenever safe interpretation is crucial and SE is not needed for specific tissue contrast enhancement.

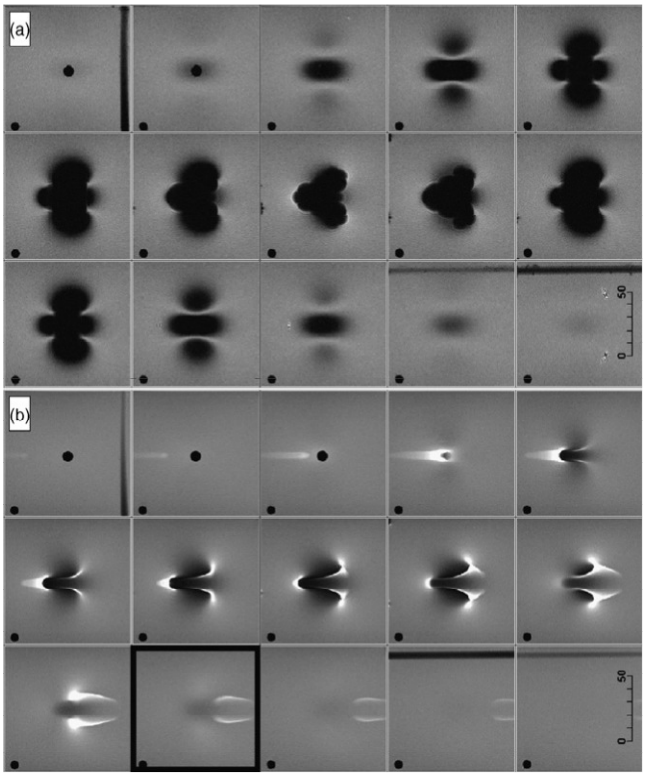

Fig. 3 – Artifacts caused by the bronze alloy NPG (Aalba Dent Inc., USA) in GE and SE MRI. The cylindrical sample was immersed in a $CuSO_4$-doped (1.25 g/L) water, oriented perpendicularly to the static magnetic field B_0 and imaged with standard imaging pulse sequences with FOV = 120 mm × 120 mm, matrix 256 × 256, slice thickness 3 mm, slice distance 6 mm. Slices are distributed symmetrically around the sample center. (a) GE: TR = 200 ms, TE = 10 ms, slice orientation "sagittal" with "PA" readout direction, flip angle 30° and (b) SE: TR = 3000 ms, TE = 15 ms, refocusing pulse flip angle 180°. The maximum distance between the sample surface to the fringe of the artifact (40.3 mm) was found in the highlighted SE slice (24 mm from the sample center).

4.4. *Material classification*

Unambiguous strict classification of metallic dental materials based on material properties only, without the specification of MRI examination parameters, the imaging region and the expected device geometry, is impossible. Obviously the acceptability of the artifact extent in orofacial MRI, where the observed area can be very close to the dental device, will be different to MR imaging of the brain and the neck, where the imaged region is further away from the device. More stringent requirements arise for shimming-sensitive methods, such as EPI or spectroscopic imaging.

4.5. *Brain and neck MRI*

It was found in the current study that all the metallic dental materials investigated that had difference susceptibility $|\chi - \chi| < 1500 \times 10^{-6}$ (amalgams, alloys of precious metals, titanium alloys, nickel–chromium alloys and cobalt–chromium alloys) can be considered MR compatible for brain and neck MRI. With some caution, the same may apply to metallic dental materials with difference susceptibility $1500 \times 10^{-6} < |\chi - \chi_{water}| < 3660 \times 10^{-6}$ (aluminum bronzes) (Fig. 4), with a slight chance of the artifact reaching the imaged area for large restorations and long-TE 2D GE.

4.6. *Orofacial MRI*

For orofacial MRI, the artifacts measured in this study by 2D GE with TE = 10 ms may be significantly reduced (more than twice) by choosing much shorter TE (such as TE = 2.65 ms, TR = 6.9 ms, flip angle 12°, shown to provide a good representation of the anatomy of this region [9]). Hence, all metallic dental materials with difference susceptibility $|\chi - \chi_{water}| < 30 \times 10^{-6}$ (amalgams and most alloys of precious metals) can be considered MR compatible. Materials with difference susceptibility $30 \times 10^{-6} < |\chi - \chi_{water}| < 200 \times 10^{-6}$ (titanium alloys and Orplid Keramik 2) will produce only limited artifacts constrained to the vicinity of the metallic device, depending on its size, shape and orientation. Materials with difference susceptibility $200 \times 10^{-6} < |\chi - \chi_{water}| < 1500 \times 10^{-6}$ (nickel–chromium and cobalt–chromium alloys) are still acceptable for observing the anatomy of the orofacial region at a suitable distance from the device. Acceptability of the materials with difference susceptibility $1500 \times 10^{-6} < |\chi - \chi_{water}| < 3660 \times 10^{-6}$ (aluminum bronzes) will depend on the geometry of the den-

Fig. 4 – Simulated overlay of the outline of the GE MR image artifact due to a sample of bronze alloy NPG (Aalba Dent Inc., USA) over a sagittal head section. The figure displays the real proportions and positions of the head and the artifact, as if the sample of the weight of a typical tooth crown was positioned at a maxillary third molar (28 or 18), i.e., in the closest position to the brain and the neck. Left-to-right as the worst-case orientation of the sample rod was assumed. GE pulse sequence as described in Fig. 3a. Under these conditions, the largest artifact would appear in the distance of approximately 8 mm from the central sagittal plane. The tooth position was estimated based on the measurements on a jaw model.

tal device and the pulse sequence used. These materials may severely affect the quality of orofacial MRI.

4.7. *Safety*

According to the literature all non-ferromagnetic materials pose either none or only negligible forces or torques [21,22] (e.g., forces and torques causing neither patient discomfort nor a danger of the device displacement), which was confirmed in this study. Heating will depend on the shape of the material and on the material's electrical conductivity [18]. No increase in temperature was subjectively felt by a volunteer with a gold crown made of the most electrically conductive material found in this study, who was MR imaged in a different study by the authors.

Acknowledgments

This study was supported by the Grant Agency of the Ministry of Health of the Czech Republic IGA MZ No. 8110-3/2004. The authors thank to Dr. Petr Krupa (St. Anne Faculty Hospital, Brno) for providing the MR system used in this study and to Dr. Karel Bartusek (Inst. Sci. Instrum., Acad. Sci. Czech Rep., Brno) for electrical conductivity measurements.

REFERENCES

[1] Schenck JF. The role of magnetic susceptibility in magnetic resonance imaging: MRI magnetic compatibility of the first and second kinds. Med Phys 1996;23:815–50.
[2] Ludeke KM, Aoschmann P, Tischler A. Susceptibility artifacts in NMR imaging. Magn Reson Imag 1985;3:329–43.
[3] Bartels LW, Smits HFM, Bakker CJG, Viergever MA. MR Imaging of vascular stents: effects of susceptibility, flow, and radiofrequency eddy currents. J Vasc Interv Radiol 2001;12:365–71.
[4] Camacho CR, Plewes DB, Henkelman RM. Nonsusceptibility artifacts due to metallic objects in MR imaging. J Magn Reson Imag 1995;5:75–88.
[5] Graf H, Steidle G, Martirosian P, Lauer UA, Schick F. Metal artifacts caused by gradient switching. Magn Reson Med 2005;54(1):231–4.
[6] Beuf O, Lissac M, Cremillieux Y, Briguet A. Correlation between magnetic resonance imaging disturbances and the magnetic susceptibility of dental materials. Dent Mater 1994;10:265–8.
[7] Lissac M, Coudert JL, Briguet A, Amiel M. Disturbances caused by dental materials in magnetic resonance imaging. Int Dent J 1992;42(4):229–33.
[8] Starčuk Z, Bartušek K, Hubálková H, Bachorec T, Starčuková J, Krupa P. Evaluation of MRI artifacts caused by metallic dental implants and classification of the dental materials in use. Meas Sci Rev 2006;6(2):24–7.
[9] Eggers G, Rieker M, Kress B, Fiebach J, Dickhaus H, Hassfeld S. Artefacts in magnetic resonance imaging caused by dental material. Magn Reson Mater Phys Biol Med 2005;18:103–11.
[10] Vikhoff B, Ribbelin S, Kohler B, Ekholm S, Borrman H. Artefacts caused by dental filling materials in MR imaging. Acta Radiol 1995;36(3):323–5.
[11] Starcuk Z, Hubalkova H, Krupa P, Bartusek K, Starcukova J, Linetskiy I. Assessment of MR compatibility of selected dental alloys. Proc Int Soc Mag Reson Med 2005;13:2276.
[12] Marques JP, Bowtell R. Numerical simulations of the DQC signal in inhomogeneous solutions. Proc Int Magn Reson Med 2003;11:1020.
[13] Balac S, Caloz G. Mathematical modeling and numerical simulation of magnetic susceptibility artifacts in Magn Reson Imag 2000; http://citeseer.ist.psu.edu/balac00mathematical.html.
[14] American Society for Testing and Materials (ASTM). F2119-01: standard test method for evaluation of MR image artifacts from passive implants. West Conshohocken, PA: ASTM International; 2001.
[15] Weglarz WP, Tanasiewicz M, Kupka T, Skorka T, Sulek Z, Jasinski A. 3D MR imaging of dental cavities—an in vitro study. Solid State Nucl Magn Reson 2004;25:84–7.
[16] Olt S, Jakob PM. Contrast-enhanced dental MRI for visualization of the teeth and jaw. Magn Reson Med 2004;52:174–6.
[17] Beuf O, Seurin MJ, Briguet A, Lissac M. Magnetic resonance imaging of rodent teeth. Magn Reson Mater Phys Biol Med 1999;8:83–6.
[18] Davis PL, Crooks L, Arakawa M, McRee R, Kaufman L, Margulls AR. Potential hazards in NMR imaging: heating effects of changing magnetic fields and RF fields on small metallic implants. AJR 1981;137:857–60.

[19] Port JP, Pomper MG. Quantification and minimization of magnetic susceptibility artifacts on GRE images. J Comput Assist Tomogr 2000;24:958–64.
[20] Hopper TAJ, Vasilic B, Pope JM, Jones CE, Epstein CL, Song HK, Wehrli FW. Experimental and computational analyses of the effects of slice distortion from a metallic sphere in an MRI phantom. Magn Reson Imag 2006;24:1077–85.
[21] New PFJ, Rosen BR, Brady TJ, et al. Potential hazards and artifacts of ferromagnetic and nonferromagnetic surgical and dental materials and devices in nuclear magnetic resonance imaging. Radiology 1983;147:139–48.
[22] Shellock FG, Monisoli S, Kanal E. MR procedures and biomedical implants, materials, and devices: 1993 update. Radiology 1993;189:587–99.